Supplementary Text

1. Evaluation against independent CO_2 observations and the global mean CGR

We evaluate the posterior fluxes indirectly by comparing the forward simulated atmospheric CO_2 concentration with independent surface flask CO_2 measurements from global background stations[1,2] (Fig. S2 and Table S1). Over the period 2015–2024, the time series of the simulated CO_2 concentrations match well the observations (Fig. S3), with the mean biases (simulations minus observations, same thereafter) being 0.25 ppm and –0.09 ppm at the global scale, and at the MLO station, respectively (Fig. S3). The magnitude and direction of the mean biases at different latitudes are similar to previous studies[3,4], which may be related to the different measurement uncertainties of the satellite at different latitudes. In 2024, the mean biases of –0.18 ppm, 0.42 ppm, and –0.73 ppm in the NH high latitudes, NH mid latitudes, and SH mid-to-high latitudes, respectively, are both within annual mean bias range for 2015–2023 and close to the average for this period (Fig. S4). Yet, we find a relatively high negative bias over the tropics (–0.37 ppm). The negative bias observed in most latitudinal bands aligns with the negative bias calculated using GCASv2 inversion-based global net carbon fluxes and global mean CGR from MBL stations (Fig. S5). Overall, our evaluations indicate that the inverted NBE fluxes may partially overestimate the land sink over the SH mid-to-high latitudes, the tropics, and the NH high latitudes, and underestimate the land sink over the NH mid latitudes in 2024.

The GCASv2 inversion-based net carbon fluxes align closely with the global mean CGR from MBL stations, with the mean bias only –0.06 ± 0.19 ppm yr^{-1} during 2015–2024 (Fig. S5). The magnitude of bias in global CGR in 2024 is comparable to that observed in 2022. The negative bias in global annual CGR between MBL observations and OCO-2-based inversions may be related to the sparsity of MBL stations[5]. To account for this limitation, we calculate the CGR from OCO-2 XCO_2 retrievals using the same methodology that is employed for MBL observations (i.e., the difference in concentration between the end of December and the start of January within each calendar year)[6]. We also find a negative bias between MBL-based CGR and OCO-2 XCO_2-based CGR (Fig. S5), although no OCO-2 observations are probably available over the NH high latitudes on 1 January and 31 December. Moreover, we use a constant conversion factor (2.086 PgC ppm^{-1}) to convert the MBL-based CGR to the whole-atmosphere mass change, assuming uniform whole-atmosphere mixing within each calendar year[7]. Yet, although the troposphere (containing ~80% of atmospheric mass) exhibits rapid mixing timescales (< 1 year), stratosphere-troposphere exchange occurs over substantially longer periods (2–4 years)[8], which may introduce error in estimating whole-atmospheric CGR. It should be noted that both MBL stations and OCO-2 observations show a record-high increase in CGR in 2024 (Fig. S5), confirming the exceptional amount of CO_2 released into the atmosphere that year.

Supplementary Figures

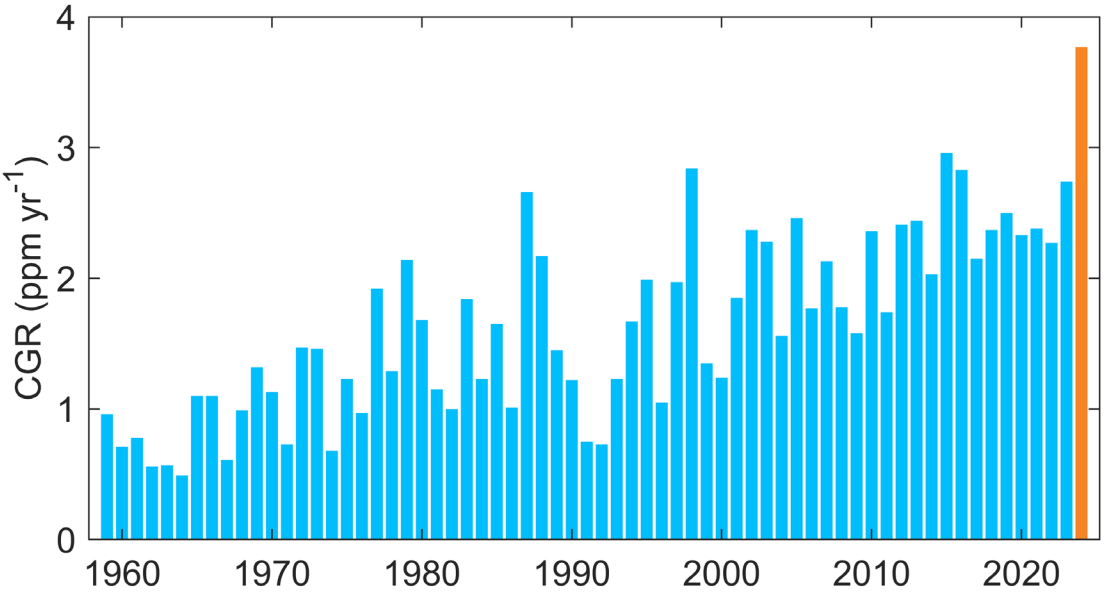

Fig. S1. Atmospheric annual mean CO_2 growth rate (CGR) from 1959 to 2024 in MBL stations from the NOAA Global Monitoring Laboratory.

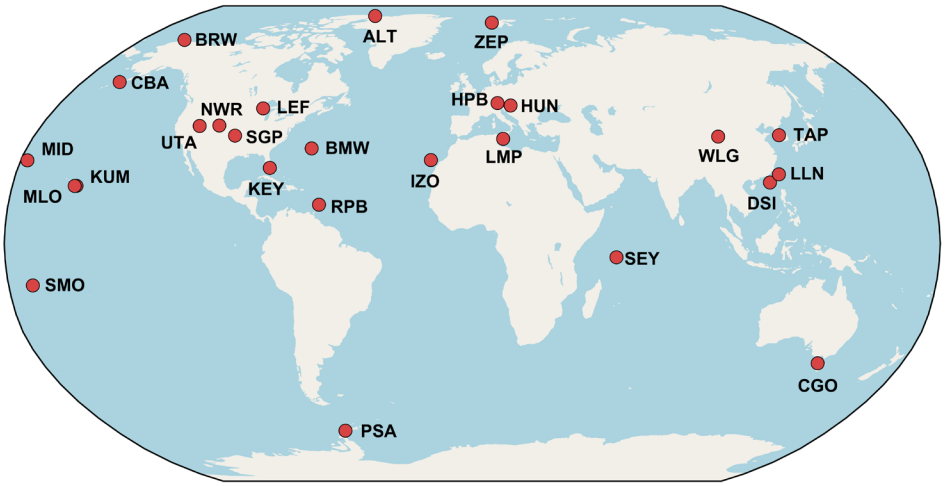

Fig. S2. Distribution of the observation sites used for independent evaluation in this study.

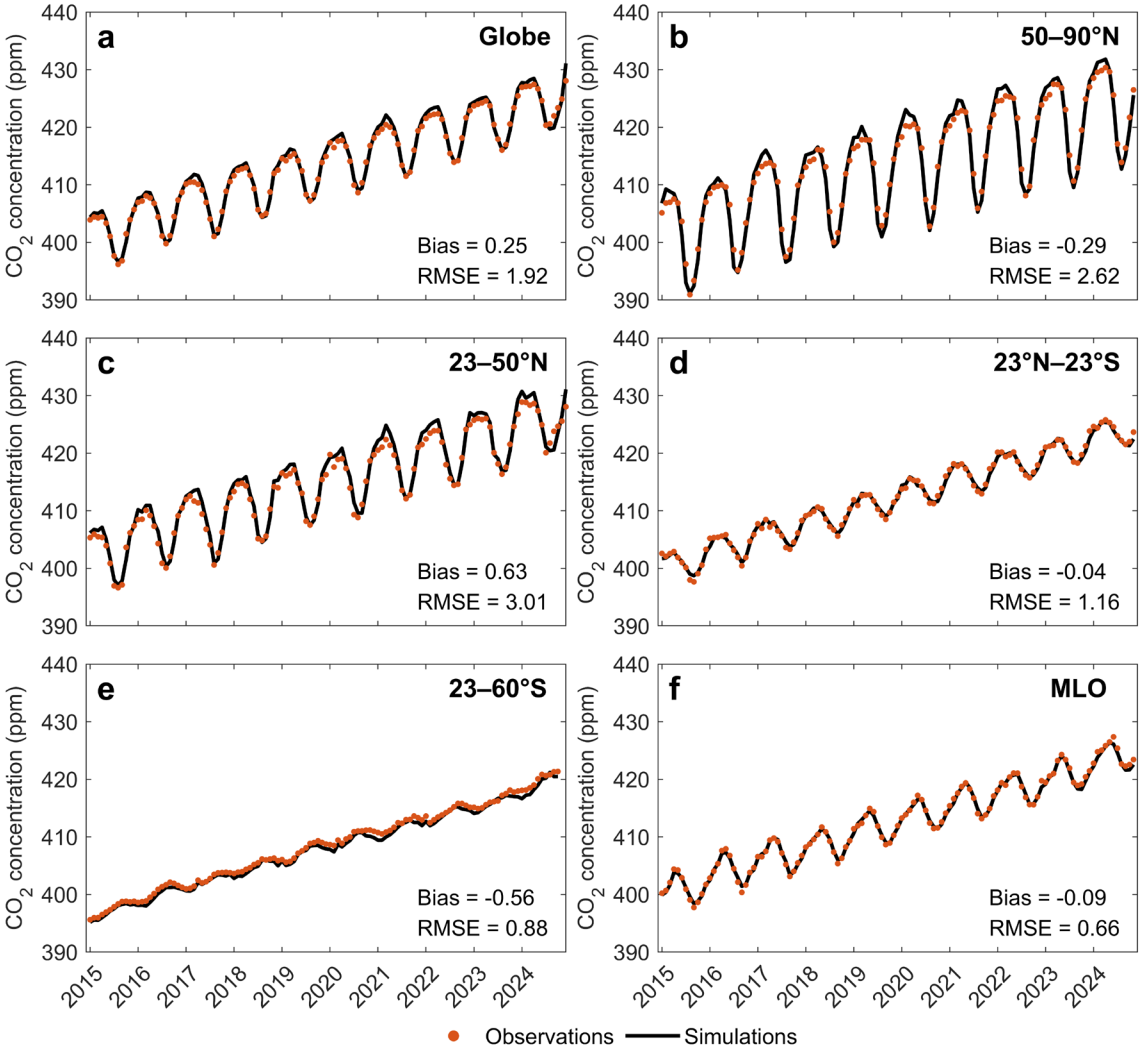

Fig. S3. Comparison between forward simulated atmospheric CO_2 concentrations and independent CO_2 observations during 2015–2024 (unit: ppm).

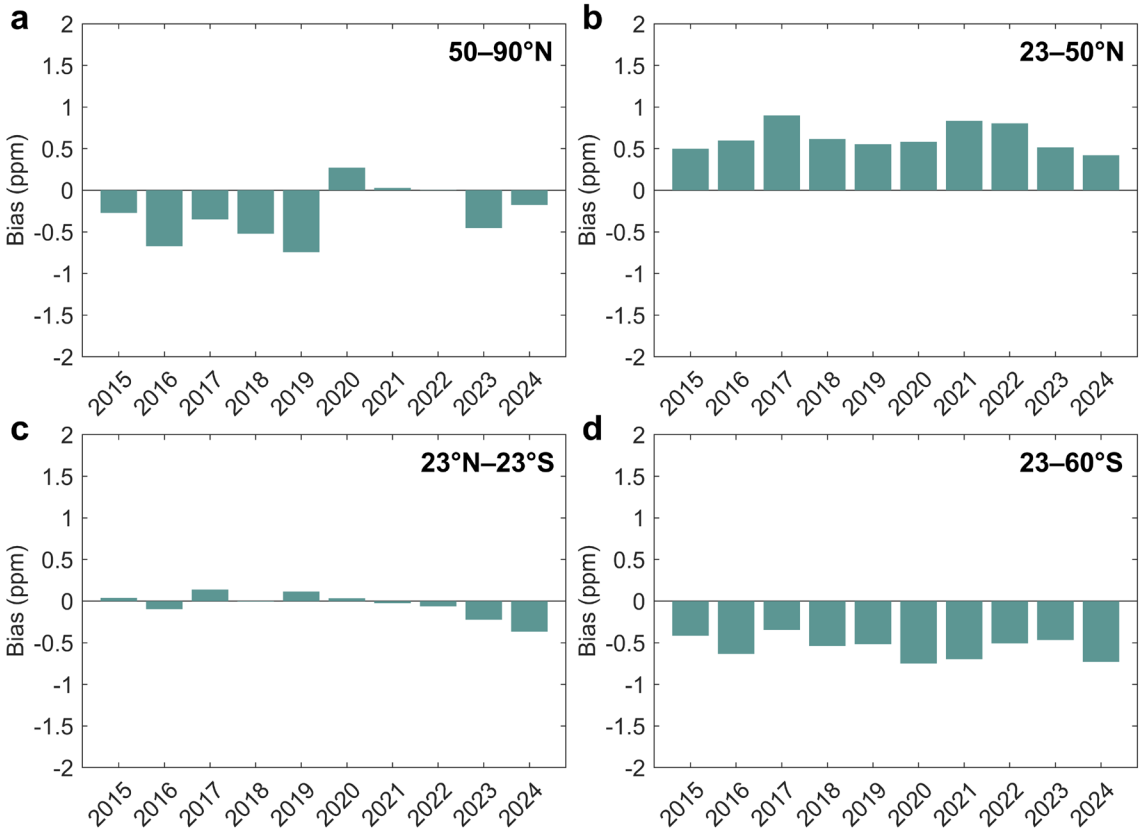

Fig. S4. Mean bias (simulations minus observations) of the evaluation during 2015–2024 for each latitudinal band (unit: ppm).

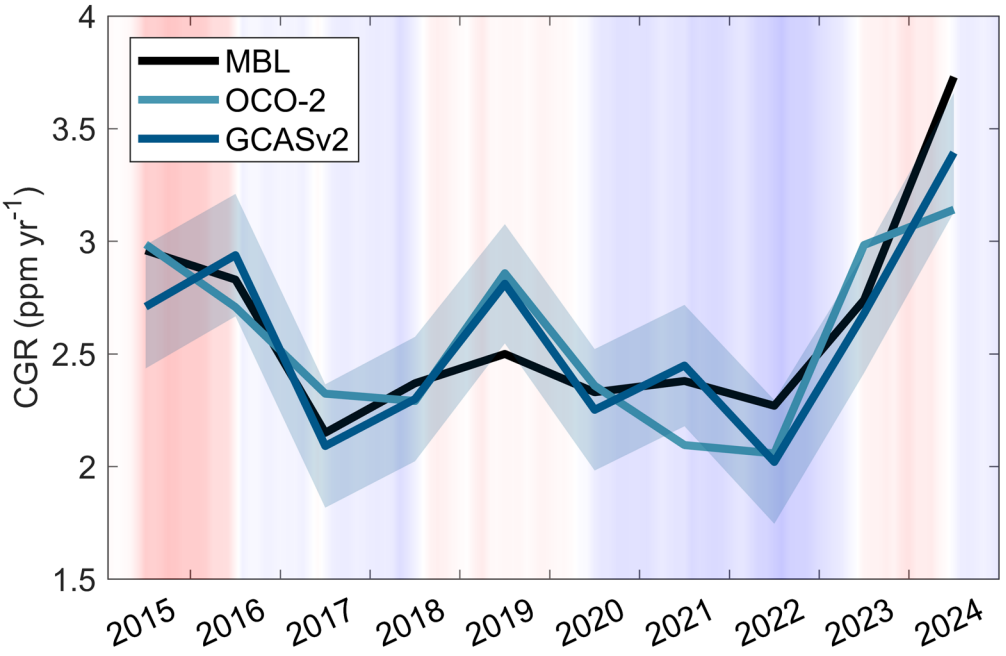

Fig. S5. Comparison between GCASv2 inversion-based global net carbon fluxes and atmospheric CO_2 growth rates (CGR) from the MBL stations and the OCO-2 XCO_2 retrievals (unit: ppm yr^{-1}). The annual global net carbon fluxes are calculated as the sum of net biosphere exchange, ocean-atmosphere carbon exchanges, and fossil fuel and cement carbon emissions, which represent the total changes of atmospheric CO_2 estimated by inversion models. The unit of net carbon fluxes (PgC yr^{-1}) was converted to the ppm yr^{-1} using the 2.086 PgC ppm^{-1} conversion factor[7]. The background color shows the intensity of El Niño (red) and La Niña (blue) events defined by MEI. Shaded areas indicate uncertainty of the inversions.

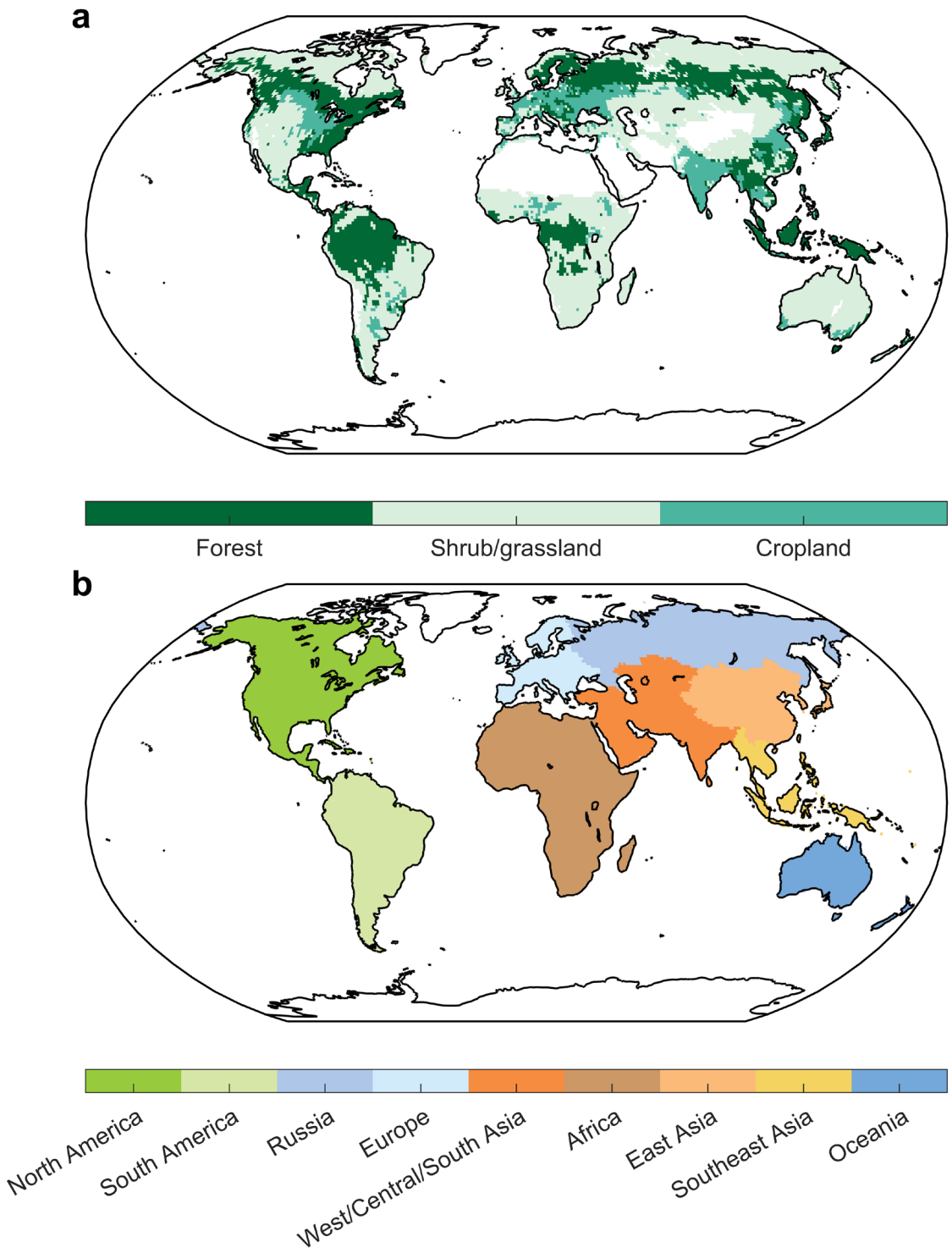

Fig. S6. Maps of (a) MODIS IGBP land cover classification and (b) the RECCAP land regions.

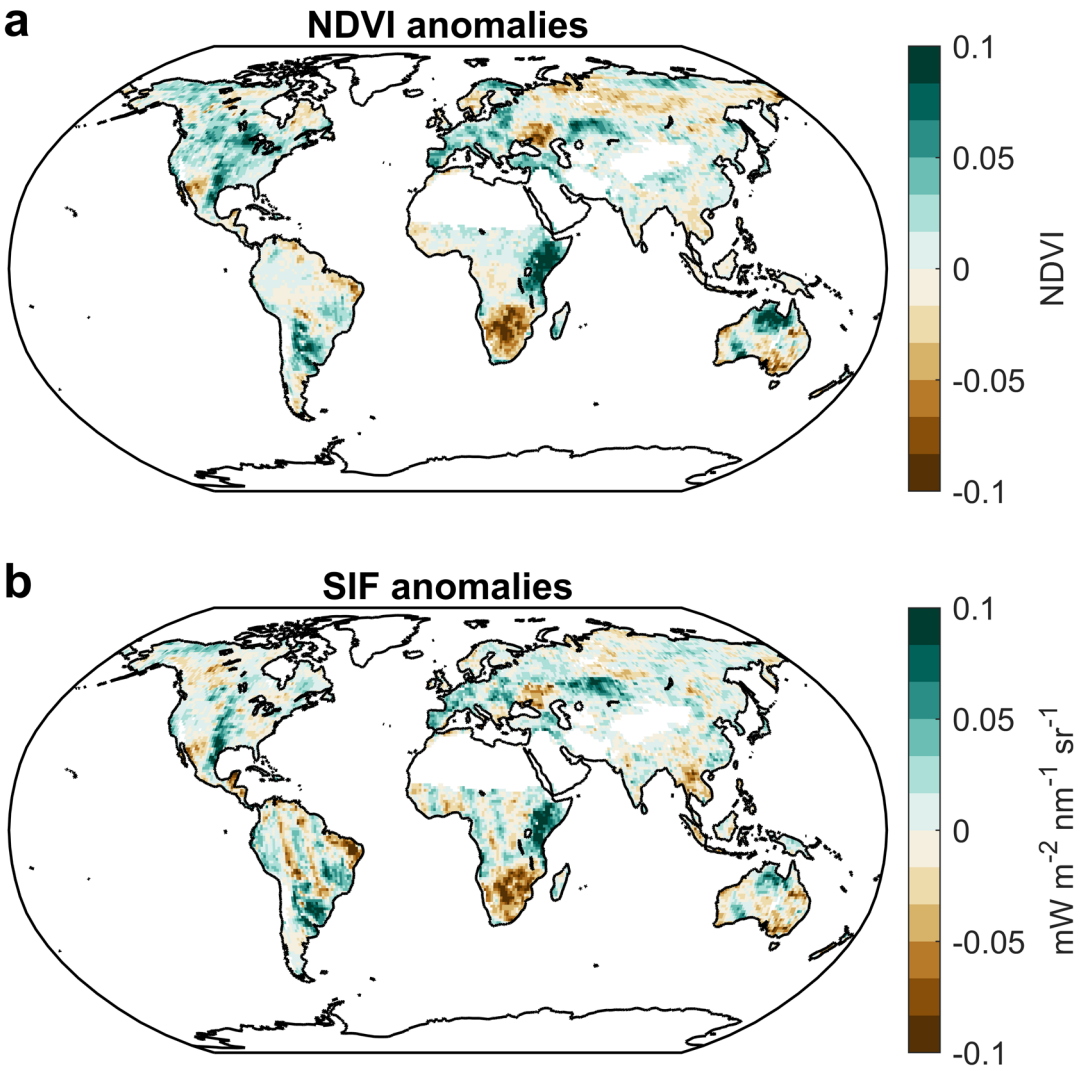

Fig. S7. Spatial patterns of normalized difference vegetation index (NDVI) and solar-induced chlorophyll fluorescence (SIF) anomalies in 2024 relative to 2022. (a) Spatial patterns of NDVI anomalies in 2024. **(b)** Spatial patterns of SIF anomalies in 2024.

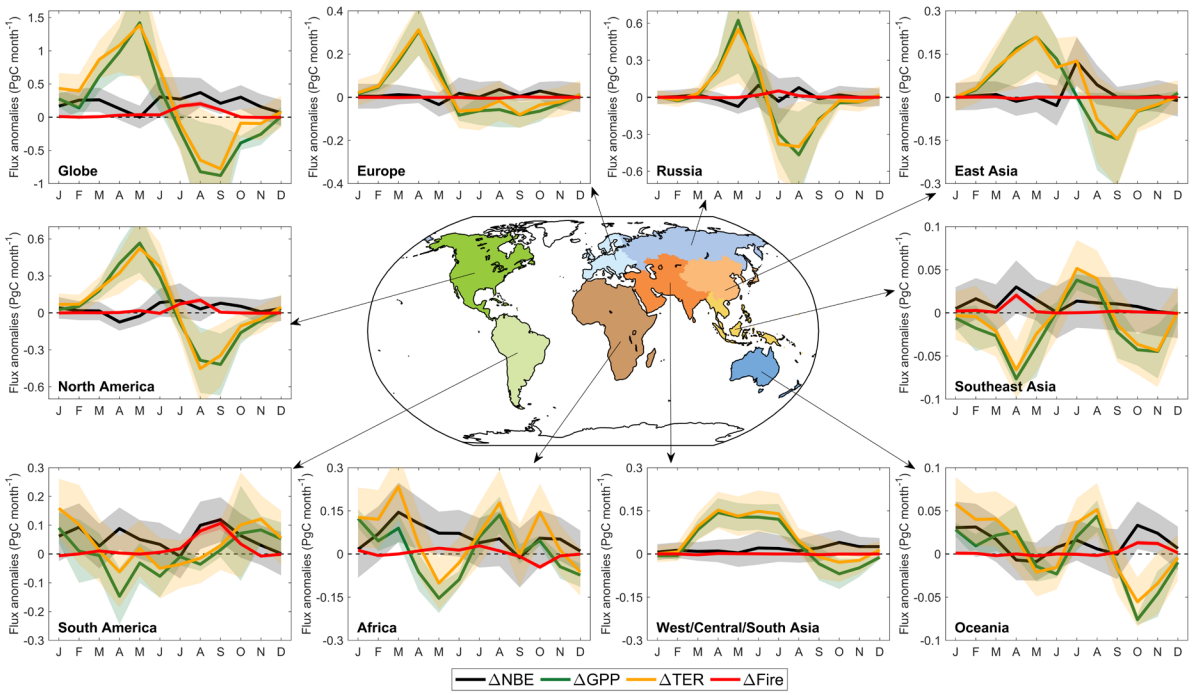

Fig. S8. Monthly anomalies of NBE, GPP, TER and wildfire emissions in 2024 in each RECCAP region (unit: PgC yr^{-1}). The shades indicate uncertainties of these carbon fluxes (see Methods).

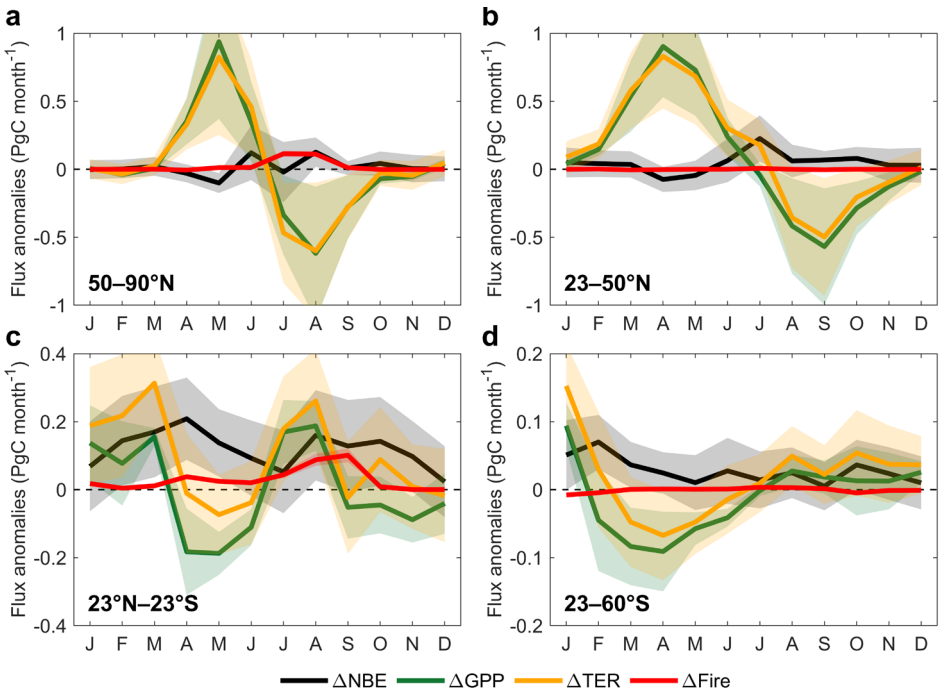

Fig. S9. Monthly anomalies of NBE, GPP, TER and wildfire emissions in 2024 over the NH high latitudes (50–90°N), NH mid latitudes (23–50°N), tropics (23°N–23°S), and SH mid-to-high latitudes (23–60°S) (unit: PgC yr^{-1}). Shaded areas indicate uncertainties of these carbon fluxes (see Methods).

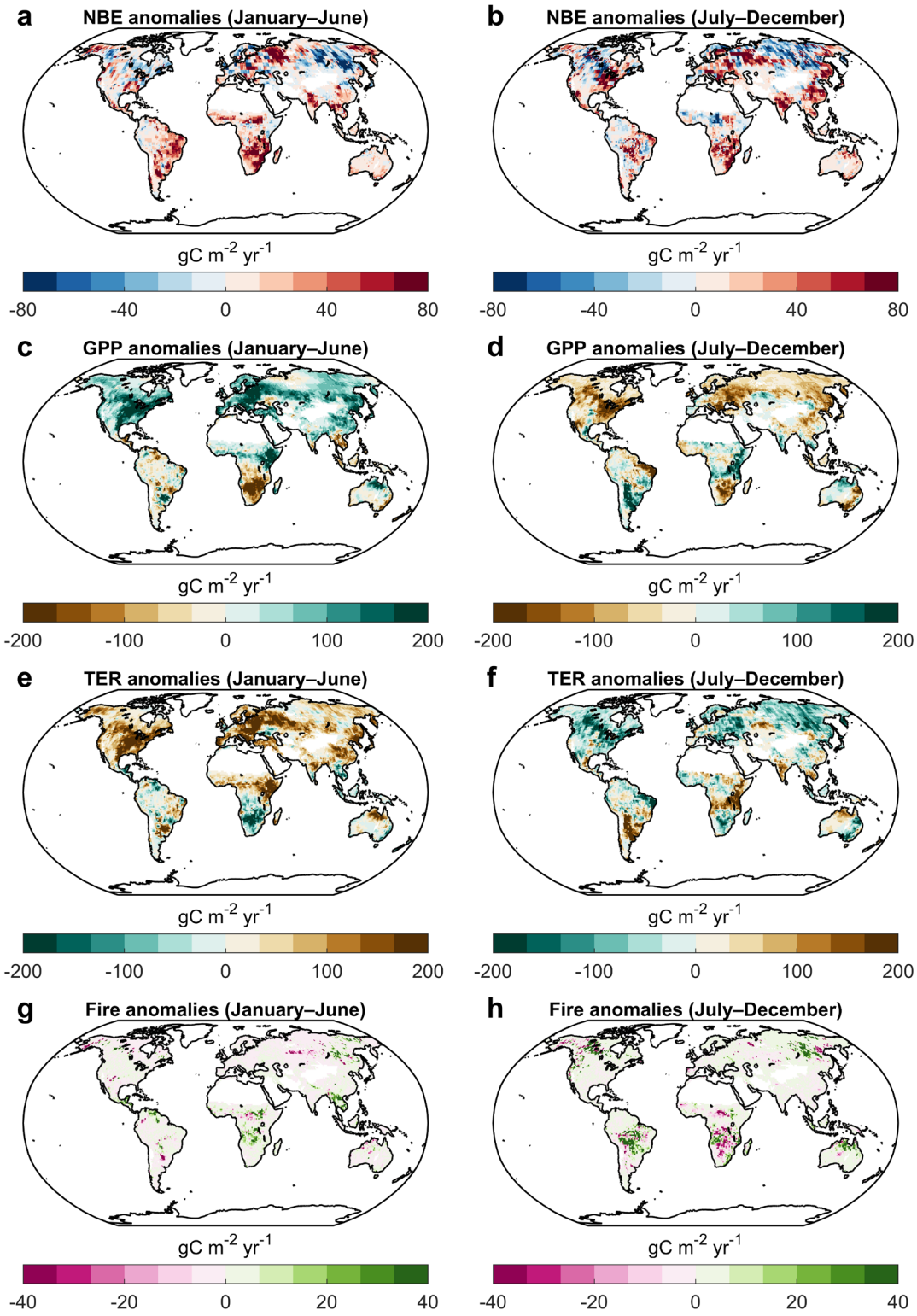

Fig. S10. Anomalies of NBE (top row), GPP (second row), TER (third row) and wildfire emissions (fourth row) over January–June (left column) and July–December (middle column) in 2024.

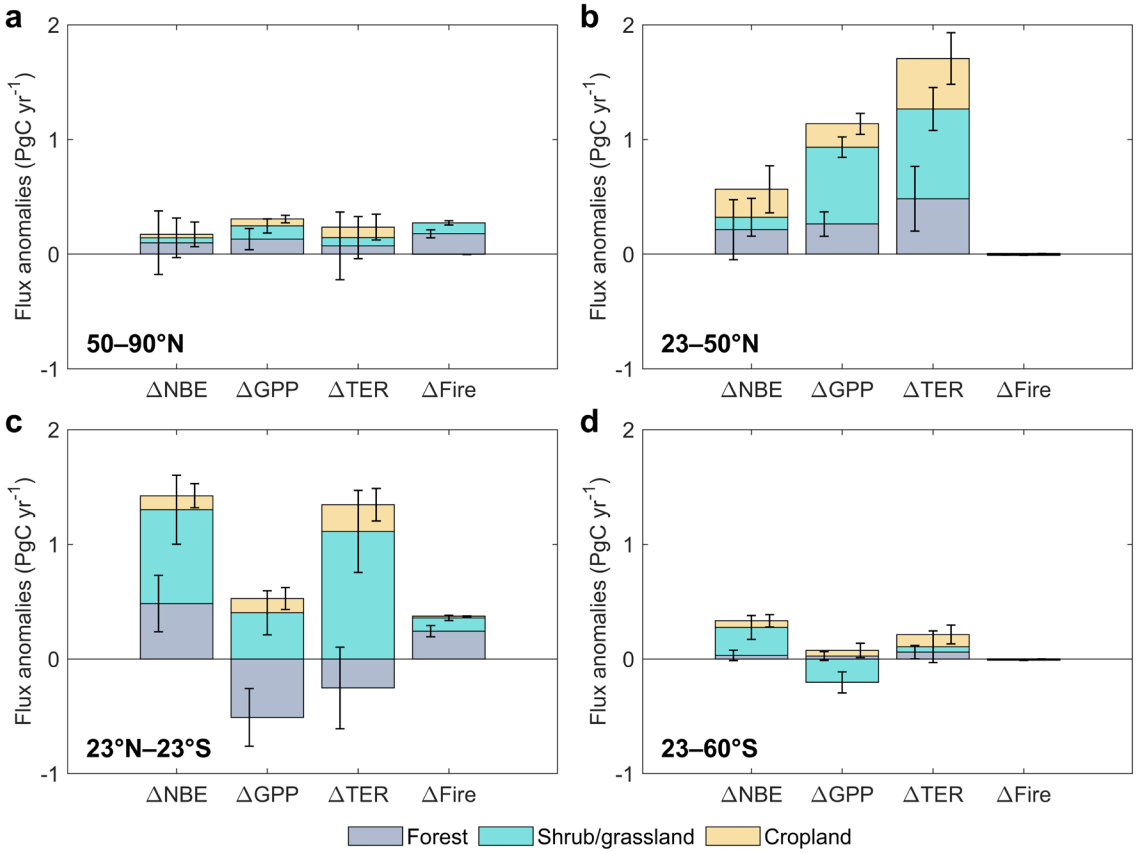

Fig. S11. Annual net biosphere exchange (NBE), gross primary production (GPP), total ecosystem respiration (TER), and wildfire emission anomalies in 2024 over forests, shrub/grasslands, and croplands in the NH high latitudes (50–90°N), NH mid latitudes (23–50°N), tropics (23°N–23°S), and SH mid-to-high latitudes (23–60°S) (unit: PgC yr^{-1}). The error bars indicate uncertainties of these carbon fluxes (see Methods).

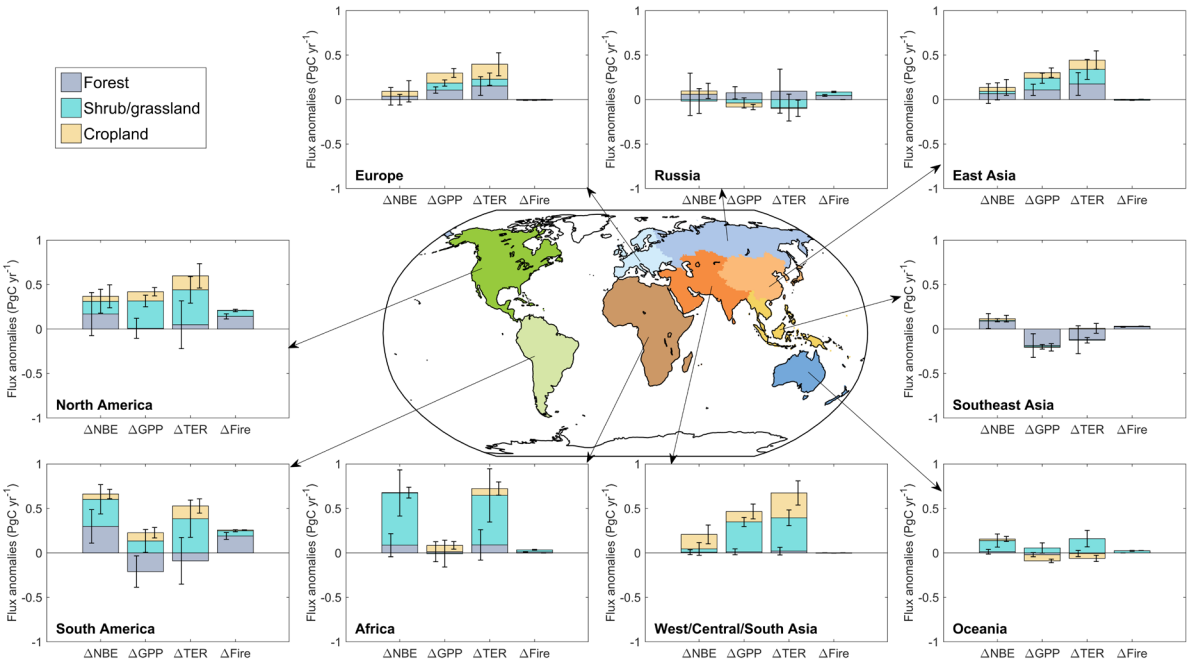

Fig. S12. Annual NBE, GPP, TER, and wildfire emission anomalies in 2024 in each RECCAP region (unit: PgC yr^{-1}). The error bars indicate uncertainties of these carbon fluxes (see Methods).

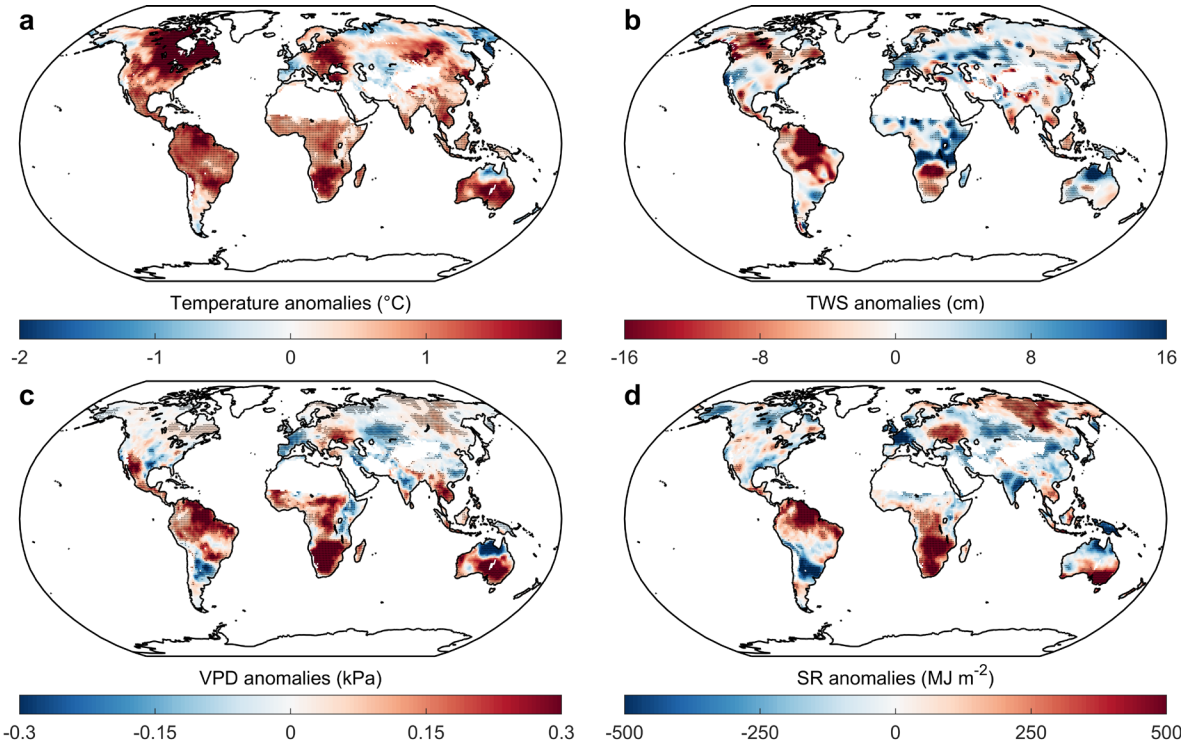

Fig. S13. Overview of global climate anomalies in 2024. (a–d) Spatial pattern of **(a)** air temperature, **(b)** terrestrial water storage (TWS), **(c)** vapor pressure deficit (VPD), and **(d)** solar radiation anomalies in 2024 relative to 2022. Black dots indicate regions with climate anomalies larger than $\sqrt{2\sigma^2}$, where σ is multi-year (2000–2021) standard deviation of the climate.

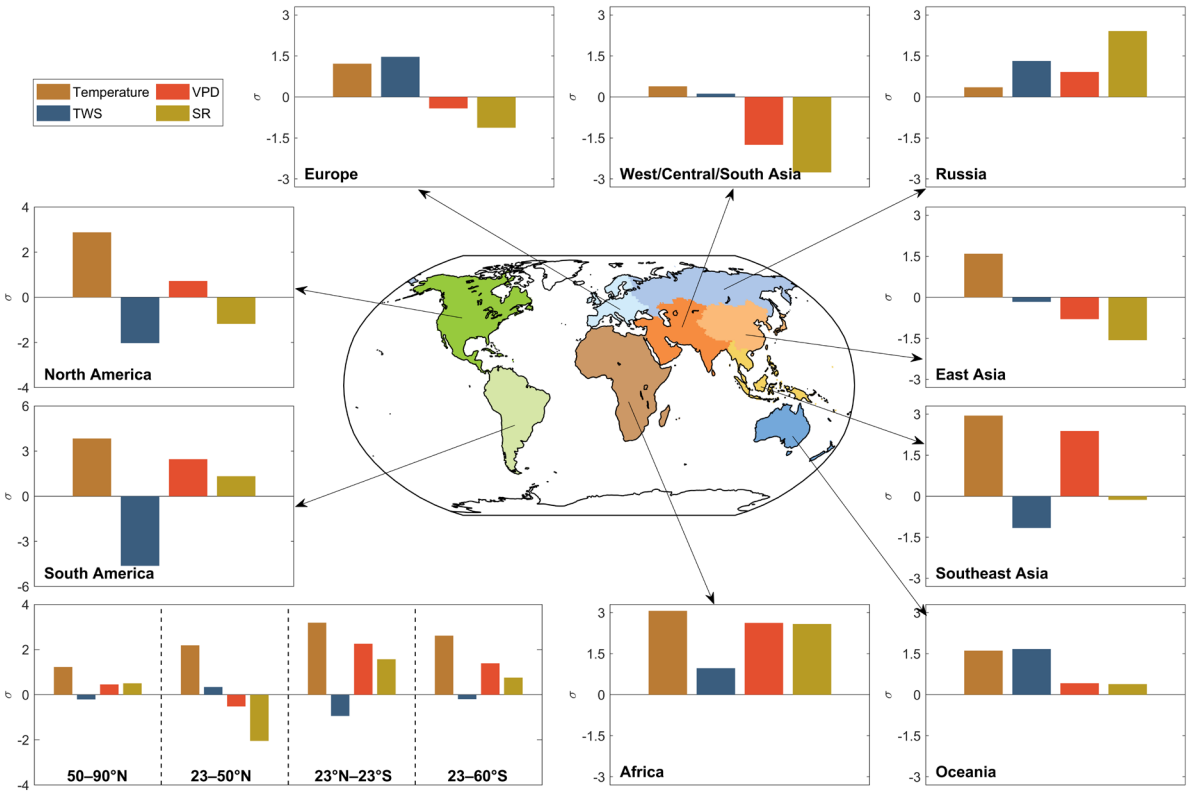

Fig. S14. Regional and latitudinal climate anomalies in 2024. The bottom left panel shows anomalies of air temperature, TWS, VPD and SR at different latitudinal bands, including NH high latitudes (50–90°N), NH mid latitudes (23–50°N), tropics (23°N–23°S), and SH mid-to-high latitudes (23–60°S). Other panels show anomalies of air temperature, TWS, VPD and SR in each RECCAP region. σ is multi-year (2000–2021) standard deviation of the climate

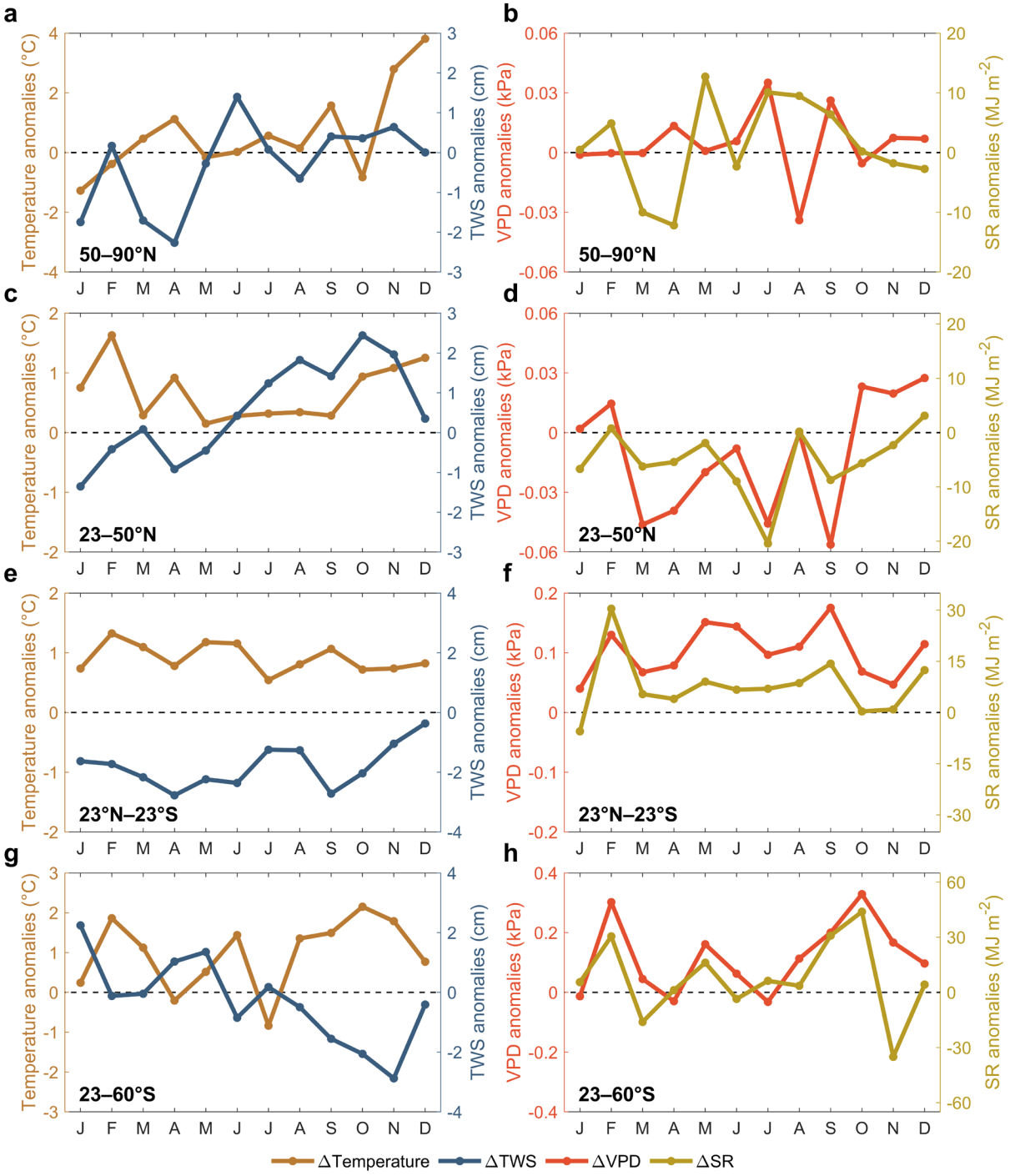

Fig. S15. Monthly anomalies of air temperature, TWS, VPD, and SR in 2024 over the NH high latitudes (50–90°N), NH mid latitudes (23–50°N), tropics (23°N–23°S), and SH mid-to-high latitudes (23–60°S).

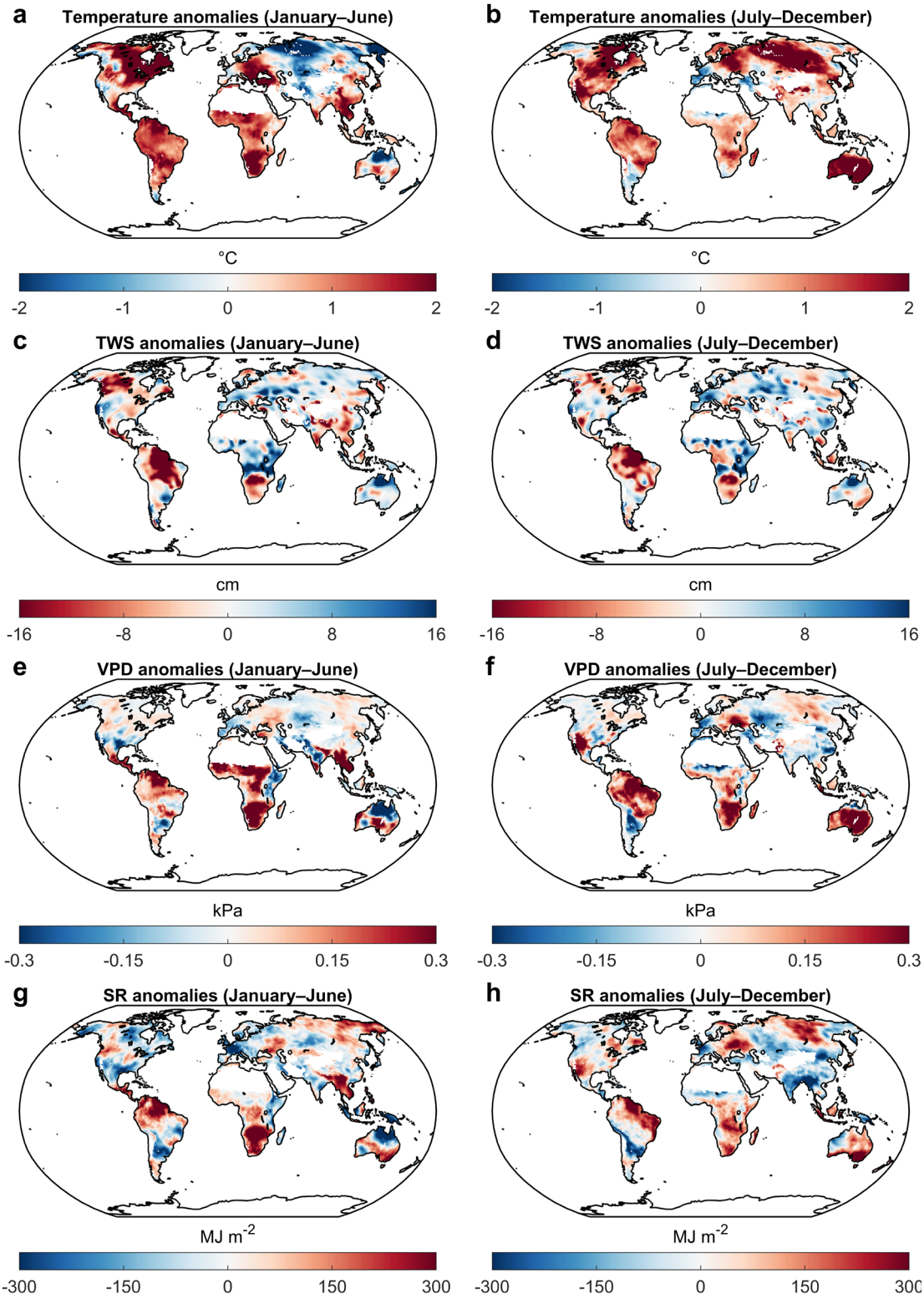

Fig. S16. Anomalies of air temperature (top row), TWS (second row), VPD (third row), and SR (fourth row) over January–June (left column) and July–December (middle column) in 2024.

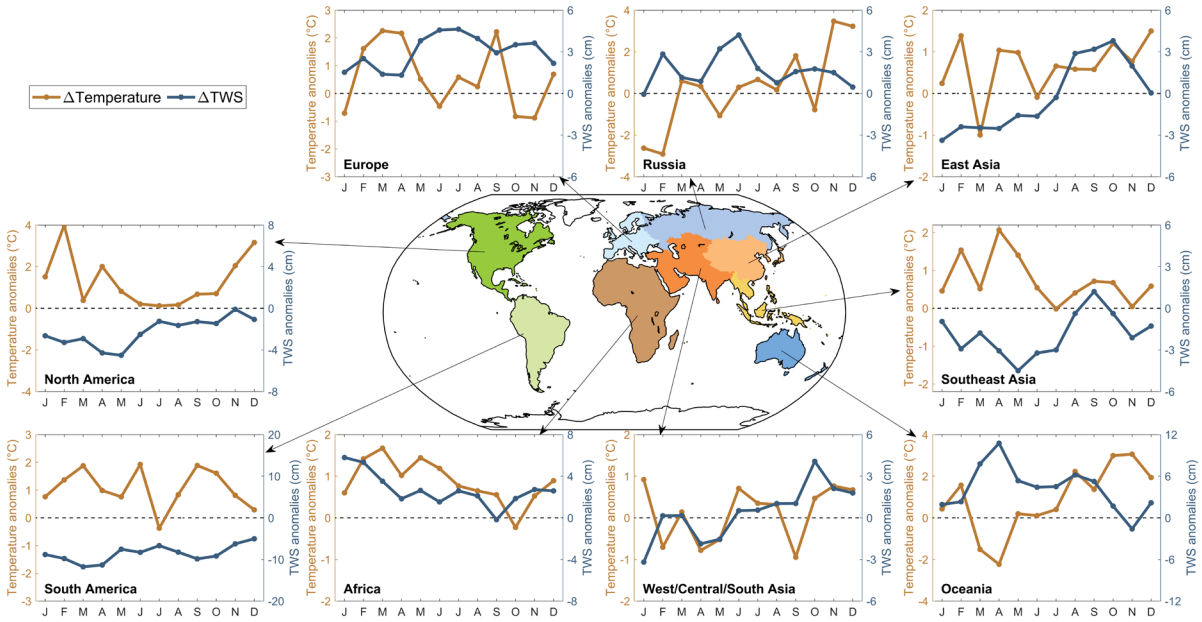

Fig. S17. Monthly anomalies of air temperature and TWS in 2024 in each RECCAP region.

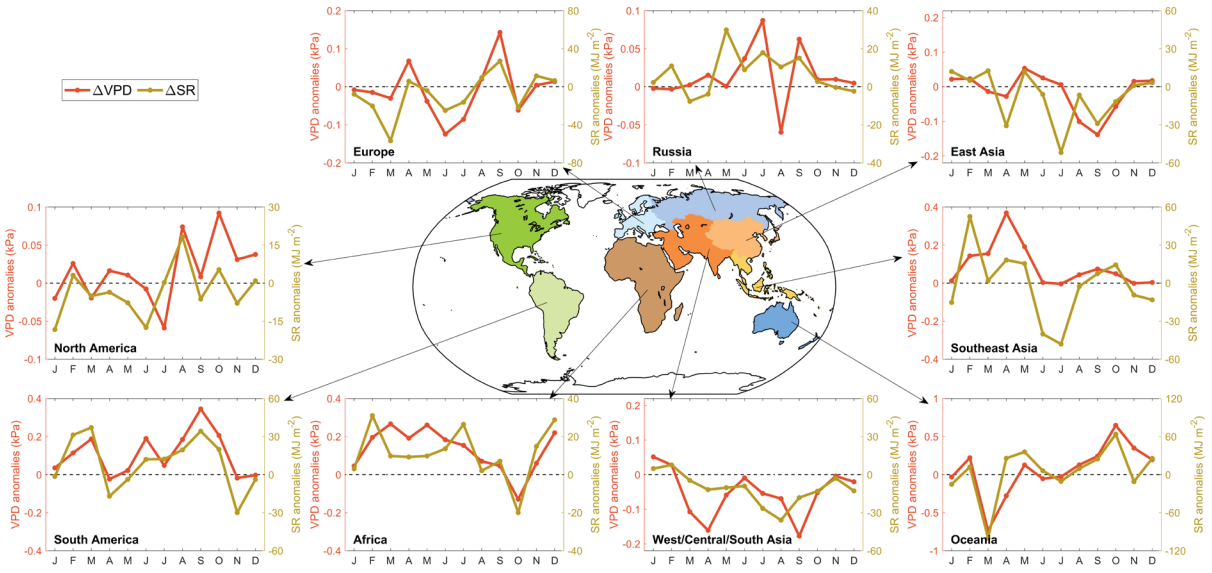

Fig. S18. Monthly anomalies of VPD and SR in 2024 in each RECCAP region.

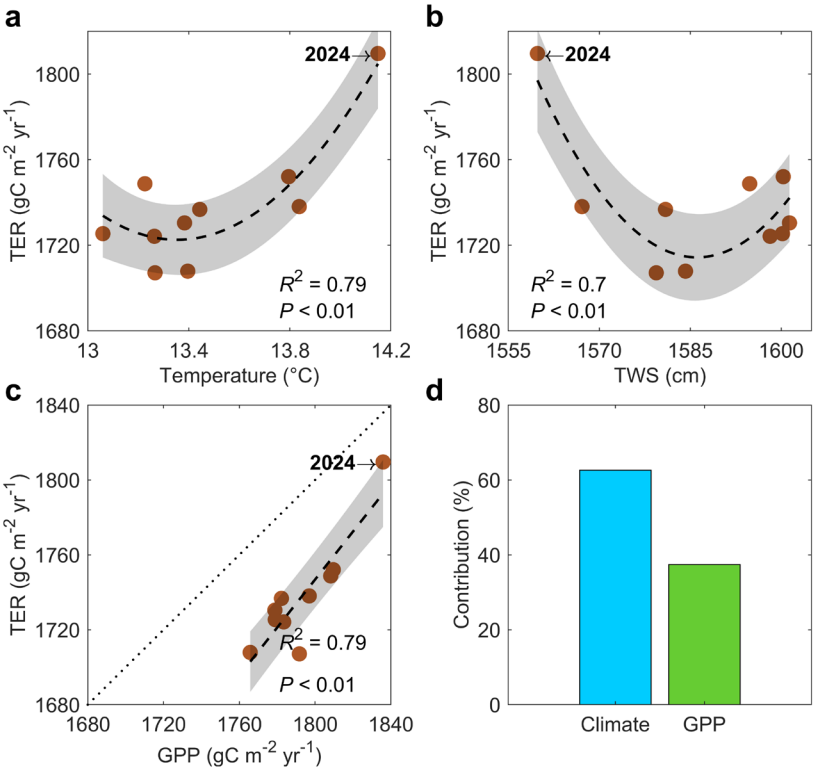

Fig. S19. The same as Fig. 5 but for forests.

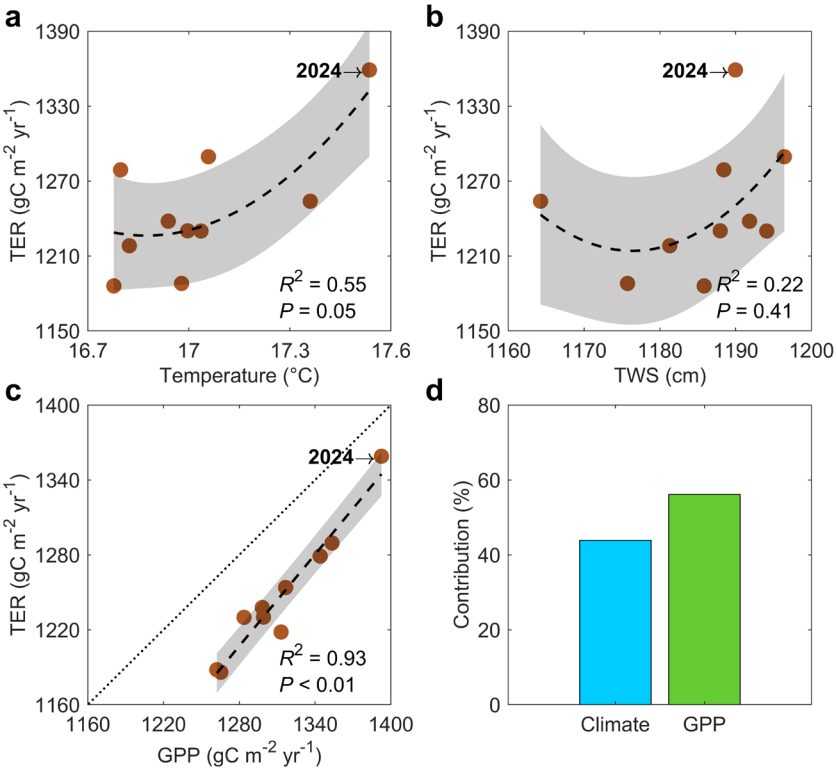

Fig. S20. The same as Fig. 5 but for croplands.

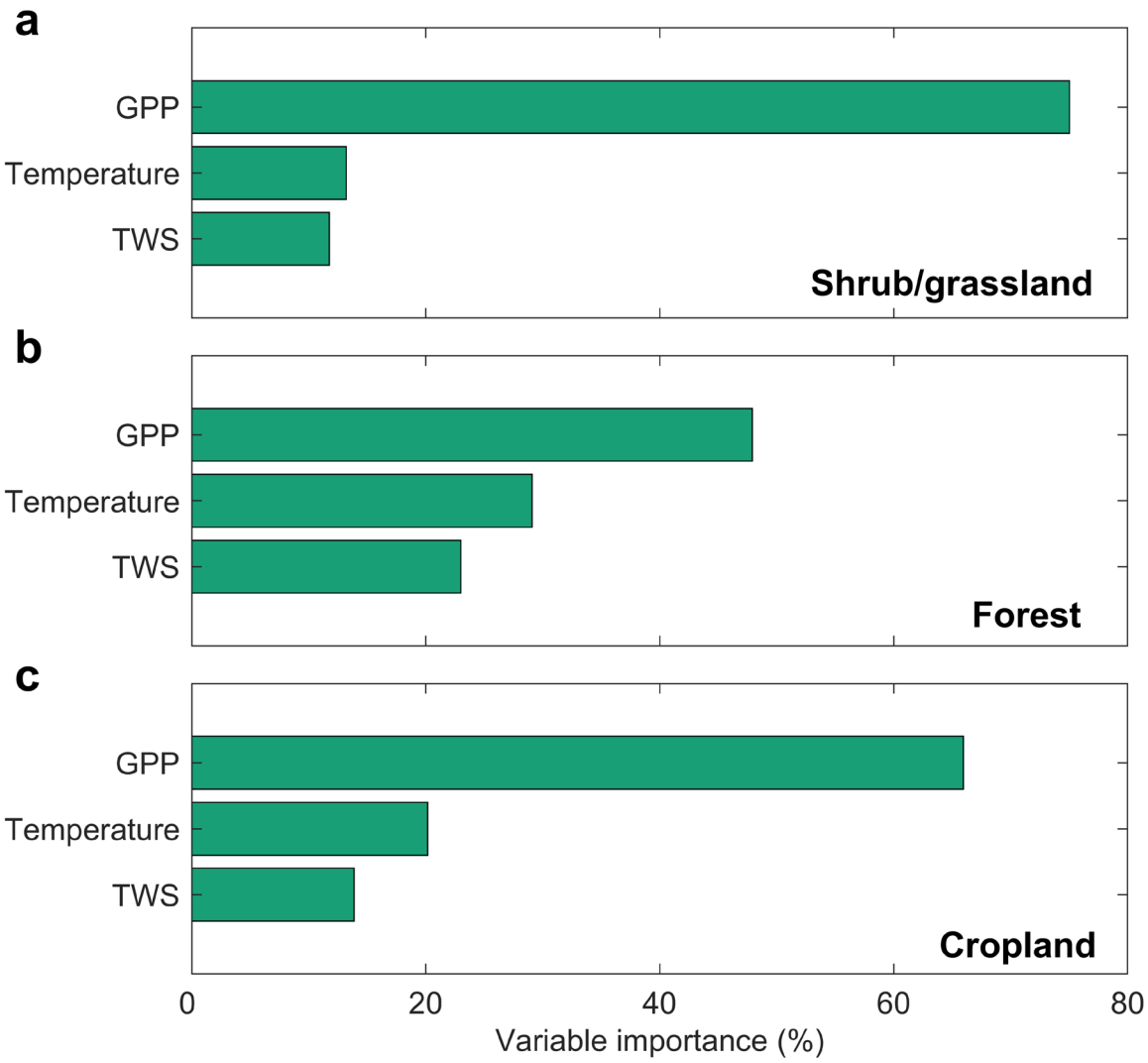

Fig. S21. Relative importance of the variables explaining the 2024 TER anomalies. The input variables include anomalies of GPP, air temperature, and TWS in 2024. High values indicate more important drivers in random forest models.

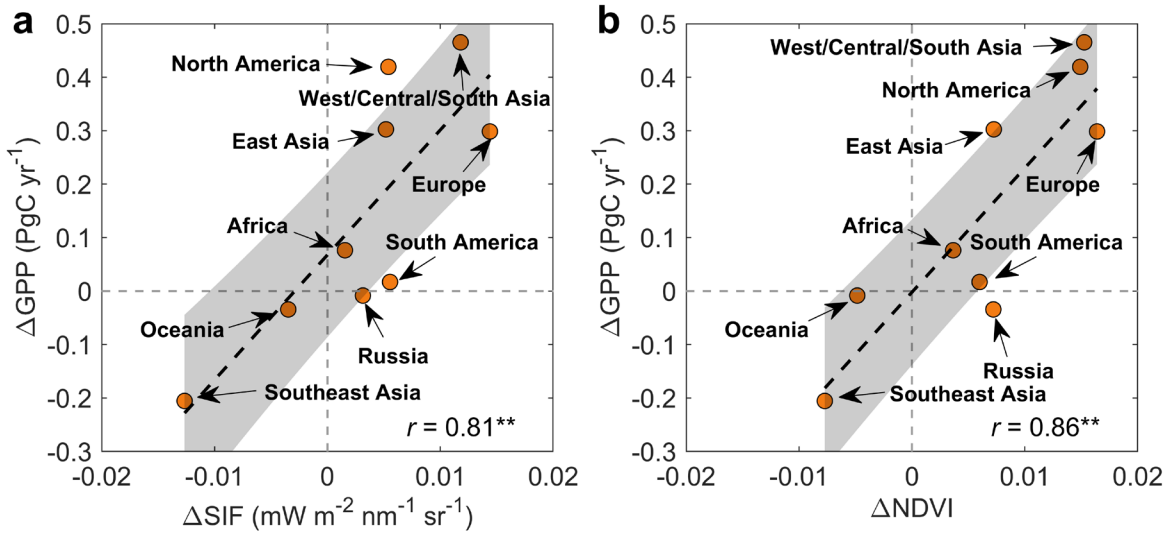

124

125 **Fig. S22. The relationship between GPP anomalies and (a) SIF and (b) NDVI anomalies**
126 **in 2024.** The orange dots represent the anomalies of GPP, SIF, and NDVI in 2024 in different
127 RECCAP regions. The black dashed lines denote the regression lines fitted to data, whereas the
128 shaded areas indicate 95% confidence interval. ** denotes $P < 0.01$.

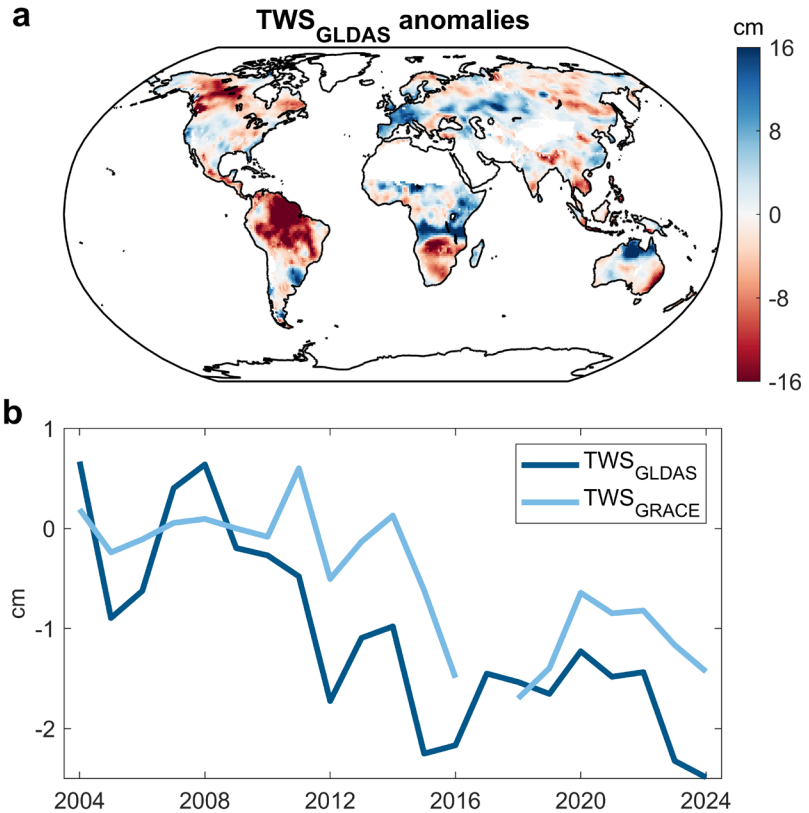

129

130 **Fig. S23. Comparison of TWS anomalies between GRACE and GLDAS products. (a)**
131 Spatial pattern of TWS anomalies for 2024 relative to 2022, calculated based on the GLDAS
132 dataset. **(b)** Time series of TWS anomalies from GRACE and GLDAS products.

Supplementary Tables

Table S1. Information for atmospheric CO_2 stations used in this study.

Site ID	Latitude	Longitude	Site name
ALT	82.451	–62.507	Alert, Nunavut, Canada
BMW	32.265	–64.879	Tudor Hill, Bermuda, United Kingdom
BRW	71.323	–156.611	Barrow Atmospheric Baseline Observatory, United States
CBA	55.210	–162.720	Cold Bay, Alaska, United States
CGO	–40.683	144.690	Cape Grim, Tasmania, Australia
DSI	20.699	116.730	Dongsha Island, Taiwan
HPB	47.801	11.024	Hohenpeissenberg, Germany
HUN	46.956	16.652	Hegyhatsal, Hungary
IZO	28.309	–16.499	Izana, Tenerife, Canary Islands, Spain
KEY	25.665	–80.158	Key Biscayne, Florida, United States
KUM	19.561	–154.888	Cape Kumukahi, Hawaii, United States
LEF	45.945	–90.273	Park Falls, Wisconsin, United States
LLN	23.470	120.870	Lulin, Taiwan
LMP	35.518	12.632	Lampedusa, Italy
MID	28.219	–177.368	Sand Island, Midway, United States
MLO	19.536	–155.576	Mauna Loa, Hawaii, United States
NWR	40.053	-105.586	Niwot Ridge, Colorado, United States
PSA	–64.774	–64.053	Palmer Station, Antarctica, United States
RPB	13.165	–59.432	Ragged Point, Barbados
SEY	–4.682	55.532	Mahe Island, Seychelles
SGP	36.607	–97.489	Southern Great Plains, Oklahoma, United States
SMO	–14.247	–170.564	Tutuila, American Samoa
TAP	36.738	126.133	Tae-ahn Peninsula, Republic of Korea
UTA	39.902	–113.718	Wendover, Utah, United States
WLG	36.288	100.896	Mt. WaliguanPeoples, Republic of China
ZEP	78.907	11.888	Ny-Alesund, Svalbard, Norway and Sweden

Table S2. Mean bias of the evaluation during 2015–2024 for each station (unit: ppm).

Site ID	2015	2016	2017	2018	2019	2020	2021	2022	2023	2024
ALT	0.66	0.51	0.30	0.35	0.78	0.52	0.10	0.36	0.29	0.30
BMW	2.65	1.10	1.59	1.64	1.69	2.44	1.53	1.82	1.49	1.09
BRW	0.16	0.17	–0.25	0.19	–0.39	–0.04	0.71	0.32	–0.14	0.20
CBA	–1.81	–2.73	–1.26	–1.86	–2.20	–0.22	–0.71	–0.60	–1.44	–0.89
CGO	–0.50	–0.77	–0.45	–0.63	–0.56	–0.88	–0.85	–0.65	–0.63	–0.80
DSI	–0.15	–0.62	0.36	0.06	0.41	–0.24	–0.19	–0.59	–0.91	–0.68
HPB	0.38	1.93	2.01	1.39	–0.08	1.92	0.94	2.47	0.82	2.84
HUN	–2.26	–1.08	–0.91	–2.03	–0.74	–3.36	0.80	0.09	0.81	0.06
IZO	0.49	0.14	0.33	0.78	0.41	0.16	0.47	0.65	0.26	–0.20
KEY	–0.21	–0.33	0.17	–0.16	–0.20	0.27	0.17	–0.69	–0.11	0.16
KUM	–0.09	–0.20	0.11	0.03	0.28	–0.08	0.10	–0.26	–0.06	–0.06
LEF	0.21	0.74	1.12	0.50	–1.06	2.24	–0.18	2.57	1.20	0.81
LLN	–0.46	–0.81	–0.39	–0.54	–0.35	–1.01	0.53	0.03	–1.00	–1.93
LMP	0.08	–0.21	0.11	–0.22	–0.13	–0.05	–0.59	–0.22	–0.76	0.16
MID	0.53	0.37	0.37	0.39	0.47	0.20	0.54	0.26	0.14	–0.22
MLO	–0.07	–0.04	0.03	0.05	–0.03	–0.09	–0.02	0.03	–0.36	–0.63
NWR	0.02	0.04	0.13	0.15	0.27	–0.17	0.02	0.60	0.33	–0.01
PSA	–0.35	–0.49	–0.25	–0.45	–0.48	–0.59	–0.57	–0.38	–0.32	–0.68
RPB	0.15	0.02	0.23	0.12	0.21	0.11	–0.10	0.28	–0.07	–0.19
SEY	0.11	–0.01	0.13	–0.20	–0.05	0.36	0.08	0.00	0.32	–0.23
SGP	0.43	1.61	0.57	1.66	1.20	1.25	1.32	0.60	0.79	1.68
SMO	–0.02	–0.02	0.08	–0.14	–0.08	–0.21	0.01	–0.08	–0.28	–0.46
TAP	2.07	2.49	4.52	1.61	1.60	2.14	4.35	2.06	1.70	0.11
UTA	2.55	3.61	2.78	2.77	2.99	2.71	3.48	3.06	2.52	2.11
WLG	0.23	0.06	0.01	0.38	0.75	1.00	1.08	0.30	0.76	0.06
ZEP	0.93	0.40	0.60	0.16	0.70	0.57	0.55	0.42	0.34	–0.04
Average	0.20	0.19	0.46	0.22	0.13	0.32	0.46	0.41	0.10	0.03

Table S3. Global carbon budget in 2024 and its anomalies relative to 2022.

Carbon flux (PgC yr^{-1})	2024	2024–2022
Fire	2.22 ± 0.44	0.65 ± 0.13
Total ecosystem respiration (TER)	140.27 ± 3.37	3.54 ± 0.88
Gross primary production (GPP)	142.66 ± 3.29	1.51 ± 0.42
Net biosphere exchange (NBE)	–0.32 ± 0.53	2.62 ± 0.76
Ocean-atmosphere carbon exchange (Ocean flux)	–2.77 ± 0.16	–0.02 ± 0.24
Fossil fuel and cement (FFC) carbon emission	10.17	0.27
Global net carbon flux (NCF)	7.08 ± 0.55	2.87 ± 0.80

References

1. Schuldt, K. N. et al. Multi-laboratory compilation of atmospheric carbon dioxide data for the period 1957-2023; obspack_co2_1_GLOBALVIEWplus_v10.1_2024-11-13 (NOAA Global Monitoring Laboratory, 2024).
2. Schuldt, K. N. et al. Multi-laboratory compilation of atmospheric carbon dioxide data for the year 2024; obspack_co2_1_NRT_v10.1_2025-02-07 (NOAA Global Monitoring Laboratory, 2024).
3. Liu, J. et al. Carbon Monitoring System Flux Net Biosphere Exchange 2020 (CMS-Flux NBE 2020). *Earth Syst. Sci. Data* **13**, 299-330 (2021).
4. Wang, H., Jiang, F., Wang, J., Ju, W. & Chen, J. M. Terrestrial ecosystem carbon flux estimated using GOSAT and OCO-2 XCO2 retrievals. *Atmospheric Chemistry and Physics.* **19**, 12067-12082 (2019).
5. Pandey, S. et al. Toward Low-Latency Estimation of Atmospheric CO2 Growth Rates Using Satellite Observations: Evaluating Sampling Errors of Satellite and In Situ Observing Approaches. *AGU Advances* **5**, e2023AV001145 (2024).
6. Lan, X., Tans, P. & Thoning, K. W. Trends in globally-averaged CO_2 determined from NOAA Global Monitoring Laboratory measurements. Version Thursday, 05-Jun-2025 08:00:43 MDT https://doi.org/10.15138/9N0H-ZH07.
7. Chevallier, F. et al. Objective evaluation of surface- and satellite-driven carbon dioxide atmospheric inversions. *Atmos. Chem. Phys.* **19**, 14233-14251 (2019).
8. Rigby, M. et al. Role of atmospheric oxidation in recent methane growth. *Proceedings of the National Academy of Sciences* **114**, 5373-5377 (2017).